Peroxisomes move by hitchhiking on early endosomes using the novel linker protein PxdA

John Salogiannis,[1] Martin J. Egan,[1] and Samara L. Reck-Peterson[1,2,3]

[1]Department of Cell Biology, Harvard Medical School, Boston, MA 02115
[2]Department of Cellular and Molecular Medicine and [3]Section of Cell and Developmental Biology, Division of Biological Sciences, University of California, San Diego, La Jolla, CA 92093

Eukaryotic cells use microtubule-based intracellular transport for the delivery of many subcellular cargos, including organelles. The canonical view of organelle transport is that organelles directly recruit molecular motors via cargo-specific adaptors. In contrast with this view, we show here that peroxisomes move by hitchhiking on early endosomes, an organelle that directly recruits the transport machinery. Using the filamentous fungus *Aspergillus nidulans* we found that hitchhiking is mediated by a novel endosome-associated linker protein, PxdA. PxdA is required for normal distribution and long-range movement of peroxisomes, but not early endosomes or nuclei. Using simultaneous time-lapse imaging, we find that early endosome-associated PxdA localizes to the leading edge of moving peroxisomes. We identify a coiled-coil region within PxdA that is necessary and sufficient for early endosome localization and peroxisome distribution and motility. These results present a new mechanism of microtubule-based organelle transport in which peroxisomes hitchhike on early endosomes and identify PxdA as the novel linker protein required for this coupling.

Introduction

Eukaryotic cells rely on the microtubule cytoskeleton to move intracellular components over long distances. Microtubules are dynamic polar structures, with "plus" ends usually located near the cell periphery and "minus" ends typically embedded in perinuclear microtubule organizing centers. Dynein motors move cargos toward the minus ends of microtubules, whereas most kinesin motors move in the opposite direction. Cytoplasmic dynein-1 (referred to here as dynein) and a relatively small number of kinesins are responsible for the transport of vesicles, organelles, proteins, and mRNAs (Vale, 2003; Cianfrocco et al., 2015).

In mammalian cells, a variety of organelles have been shown to depend on dynein and kinesin for transport, including endosomes, mitochondria, peroxisomes, Golgi, endoplasmic reticulum, autophagosomes, lysosomes, and nuclei (Harada et al., 1998; Tanaka et al., 1998; Roghi and Allan, 1999; Schrader et al., 2000; Kural et al., 2005; Maday and Holzbaur, 2012; Neuhaus et al., 2015). In some cases, the adaptors that link the molecular motors to their cargos have been identified (Kardon and Vale, 2009; Fu and Holzbaur, 2014; Cianfrocco et al., 2015). For example, in the case of mitochondria, TRAK/Milton proteins recruit kinesin-1 and dynein (Glater et al., 2006; Wang and Schwarz, 2009; van Spronsen et al., 2013), and in the case of early endosomes (EEs), Hook proteins have been shown to recruit dynein and kinesin-3 (Bielska et al., 2014; Zhang et al., 2014). This has led to the idea that each type of cargo uses distinct machinery to recruit molecular motors. Our goal is to use the model fungus *Aspergillus nidulans* to identify how different cargos engage the transport machinery.

A. nidulans and other filamentous fungi have proven to be excellent model systems for studying microtubule-based transport (Egan et al., 2012a). In these fungi, microtubules are used to transport cellular cargos through highly polarized, multinucleate cells, called hyphae. Furthermore, rapid forward genetics are possible, and genome engineering is fast and simple (Horio and Oakley, 2005; Nayak et al., 2006). In *A. nidulans*, microtubules are uniformly polarized from the hyphal tip to the tip-proximal nucleus, such that plus ends are located at hyphal tips and minus ends are embedded in the nuclear membrane (Egan et al., 2012b). As a result of this organization, defects in dynein-mediated transport generally lead to accumulation of cargo at the hyphal tip, whereas defects in kinesin-3/UncA transport can cause accumulation of cargo at the tip-proximal nucleus (Fig. 1; Egan et al., 2012a).

We took advantage of these clear organelle distribution phenotypes to conduct a forward genetic screen in *A. nidulans* to identify novel genes required for the microtubule-based movement of dynein and kinesin cargos (Tan et al., 2014). For our screen, we focused on three well-characterized cargos of dynein and kinesin: EEs, peroxisomes, and nuclei (Xiang et al.,

Correspondence to Samara L. Reck-Peterson: sreckpeterson@ucsd.edu

Abbreviations used in this paper: CC, coiled-coil domain; EE, early endosome; FL, full-length; PTS1, peroxisome targeting signal 1; UR, uncharacterized region; WT, wild-type.

The Rockefeller University Press $30.00
J. Cell Biol. Vol. 212 No. 3 289–296
www.jcb.org/cgi/doi/10.1083/jcb.201512020

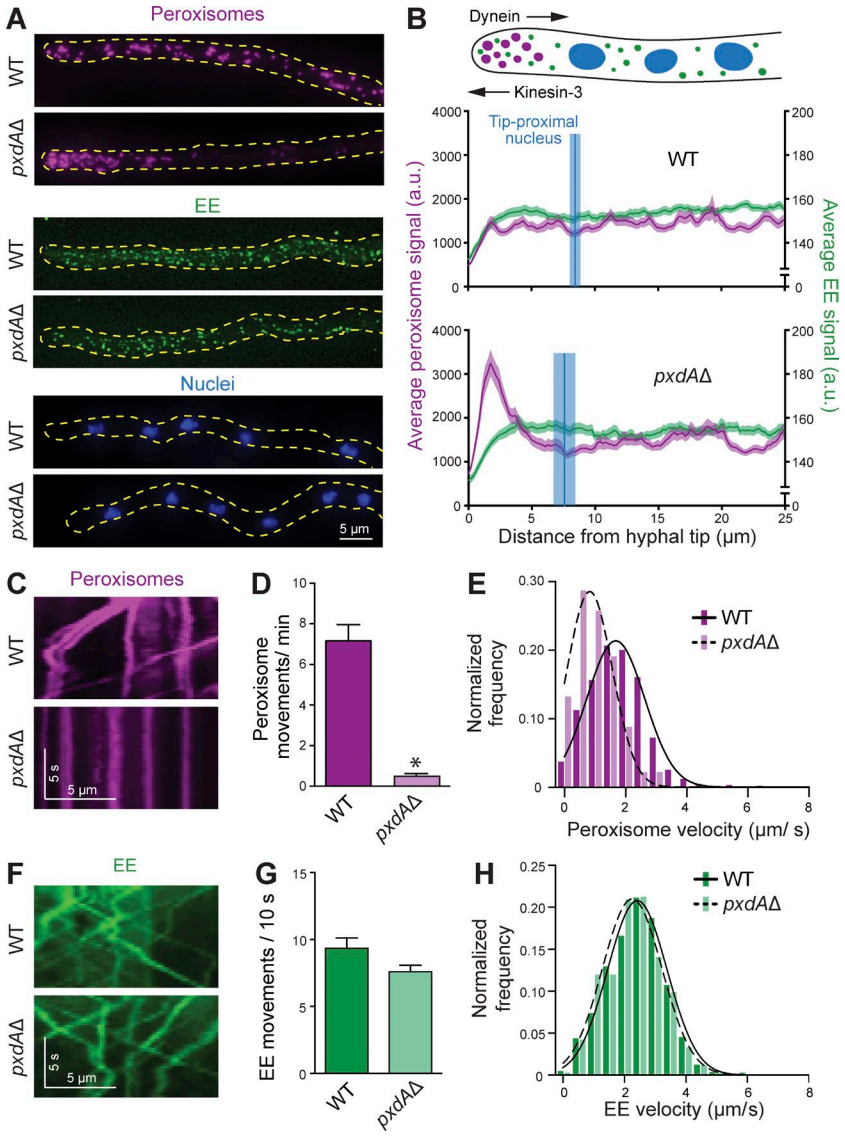

Figure 1. ***pxdA* is required for the distribution and movement of peroxisomes, but not EEs or nuclei.** (A) Representative micrographs of WT and *pxdAΔ* hyphae expressing fluorescent proteins that label peroxisomes (mCherry-PTS1), EEs (GFP-RabA/5a) or nuclei (Histone H1–TagGFP). (B) Cartoon of an *A. nidulans* hypha (top). Dynein moves away from the hyphal tip, whereas kinesin-3 moves in the opposite direction. Peroxisome (magenta) and EE (green) distribution in hyphae was quantified from line scans of fluorescence micrographs and displayed as the mean (solid lines) ± SEM (shading) fluorescence intensity as a function of distance from the hyphal tip. Peroxisome distribution near the hyphal tip was significantly different between WT and *pxdAΔ* ($P < 0.001$, two-way analysis of variance, Bonferroni post hoc test significant between 0.65 and 3.25 µm from hyphal tip; $n = 40$ hyphae [WT] and $n = 44$ [*pxdAΔ*]). EE distribution was not significantly different between WT and *pxdAΔ* ($P = 0.99$, two-way analysis of variance; $n = 51$ hyphae [WT] and $n = 33$ [*pxdAΔ*]). Nuclear distribution was quantified by measuring the distance from the tip-proximal nucleus to the hyphal tip. The mean (blue vertical lines) ± SEM (blue shading) was 8.47 ± 0.39 µm in WT and 7.66 ± 0.42 µm in *pxdAΔ* hyphae. The means were not significantly different between WT and *pxdAΔ* ($P = 0.1073$, Mann-Whitney test; $n = 31$ hyphae [WT] and $n = 31$ [*pxdAΔ*]). (C) Representative kymographs generated from movies of peroxisomes in WT and *pxdΔ* hyphae. (D) Bar graph of the flux of peroxisome movements in WT and *pxdAΔ* hyphae, calculated as the number of peroxisomes crossing a line drawn perpendicular and 10 µm away from the hyphal tip during a 1-min time-lapse movie. Peroxisome movements were 7.17 ± 0.79 (SEM) per minute in WT and 0.52 ± 0.10 per minute in *pxdAΔ* hyphae (*, $P < 0.0001$, Mann-Whitney test; $n = 44$ hyphae for both genotypes). (E) Histogram of instantaneous velocities of moving peroxisomes in WT versus *pxdAΔ* strains. Mean velocities were 1.75 ± 0.99 (SD) µm/s in WT and 0.97 ± 0.68 µm/s in *pxdAΔ* hyphae ($P < 0.001$, Kolmogorov-Smirnov test; $n = 1,195$ instantaneous velocities [WT] and $n = 136$ [*pxdAΔ*]). (F) Kymographs generated from movies of EEs in WT and *pxdAΔ* hyphae. (G) Bar graph of the flux of EE movements during a 10-s movie calculated as in D. EE movements were 9.34 ± 0.78 (SEM) per min in WT and 7.60 ± 0.48 per min in *pxdAΔ* hyphae ($P = 0.0920$, Mann-Whitney test; $n = 29$ hyphae [WT] and $n = 47$ hyphae [*pxdAΔ*]). (H) Histogram of instantaneous velocities of EEs in WT versus *pxdAΔ* strains. Mean velocities are 2.40 ± 0.99 (SD) µm/s in WT and 2.24 ± 0.93 µm/s in *pxdAΔ* hyphae ($P = 0.0274$, Kolmogorov-Smirnov test; $n = 1,602$ instantaneous velocities [WT] and $n = 332$ [*pxdAΔ*]).

1994; Wedlich-Söldner et al., 2002; Abenza et al., 2009; Egan et al., 2012b). We identified novel alleles of known components of the transport machinery and many genes not previously connected to transport (Tan et al., 2014). One expectation was that some of these novel genes would encode organelle-specific adaptors for dynein or kinesin.

In this study, we focused on hits from our screen that caused peroxisome-specific phenotypes. Peroxisomes are responsible for the β-oxidation of long-chain fatty acids and guard against toxic reactive oxygen species (Liu et al., 2008). Their microtubule-based motility is likely important to achieve even distribution in the cell (Neuhaus et al., 2015). We identified a novel coiled-coil–containing protein, PxdA, that is required for the distribution and long-range movement of peroxisomes. We show that PxdA colocalizes with EEs and that its EE localization is required for peroxisome movement. We find that both PxdA and EEs co-migrate with moving peroxisomes. Recently, it was reported that peroxisomes and other cargo could "hitchhike" on EEs in the plant pathogenic fungus *Ustilago maydis* to achieve long-range movement (Baumann et al., 2012; Higuchi et al., 2014; Guimaraes et al., 2015), but the molecules mediating this behavior were not known. Our data demonstrate that PxdA is a novel linker protein mediating peroxisomal hitchhiking on EEs.

Results and discussion

PxdA is a novel protein required for peroxisome distribution and motility

In our original screen, 19 mutants were categorized as only affecting peroxisome distribution, making them excellent candidates for cargo-specific regulators (Tan et al., 2014). Whole-genome sequencing of two mutants (RPA604 and RPA628) with a strong peroxisome distribution phenotype identified independent mutations in the uncharacterized gene AN1156; both mutations were predicted to result in premature stop codons. AN1156 mutants displayed hyphal tip accumulation of peroxisomes, but normal distribution of RabA/5a-positive EEs

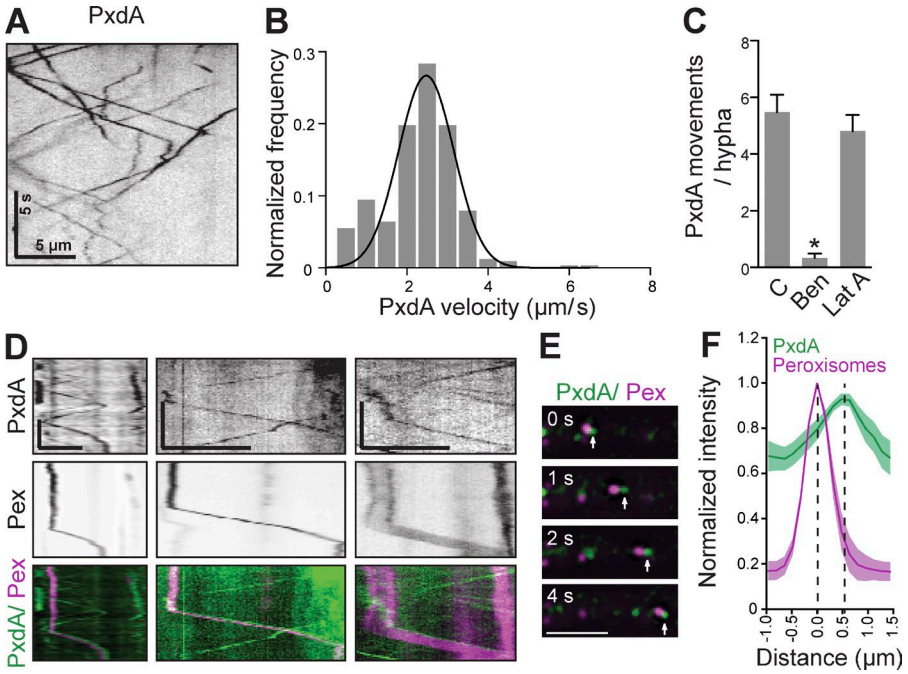

Figure 2. **Microtubule-based movement of PxdA colocalizes with moving peroxisomes.** (A) Representative kymograph generated from a movie of PxdA-GFP. (B) Histogram of velocities calculated from PxdA-GFP and PxdA-mKate kymographs. Mean velocity is 2.32 ± 0.88 (SD; n = 328). (C) Bar graph of the number of PxdA-mKate movements calculated as the number of puncta crossing a line drawn perpendicular to the hyphal long axis during a 10-s movie. PxdA puncta moved 5.48 ± 0.62 (SEM) per hyphae in the DMSO control (C; n = 21 hyphae), 0.33 ± 0.16 per hyphae in the presence of benomyl (Ben; n = 15), and 4.81 ± 0.57 per hyphae in the presence of latrunculin A (Lat A; n = 16). Benomyl but not latrunculin A treatment was significantly different than the control (one-way analysis of variance, Bonferroni post hoc test, *, P < 0.001). (D) Representative kymographs generated from simultaneous time-lapse movies of peroxisomes (Pex) and PxdA-GFP. 65.6% (n = 29) of moving peroxisomes overlapped with PxdA. Bars: (x axis) 5 µm; (y axis) 5 s. Left panels correspond to Video 5. (E) Stills from Video 6 of peroxisomes (Pex) and PxdA-GFP. White arrows point to a co-migrating PxdA puncta and peroxisome. Bar, 5 µm. (F) Normalized intensity line scans of peroxisomes and PxdA during comigrating runs (n = 11).

and nuclei (Fig. S1 A). Based on this phenotype, we named AN1156 *pxdA* (peroxisome distribution mutant A). To confirm that PxdA is expressed, we performed immunoblots of lysates from an HA-tagged *pxdA* strain and detected an ∼250-kD band (Fig. S1 B), which corresponds well to the larger of two predicted open reading frames for AN1156.

To verify that *pxdA* plays a role in regulating peroxisome distribution, we deleted the endogenous gene in haploid strains containing fluorescently labeled EEs, peroxisomes, or nuclei. Consistent with the phenotype of RPA604 and RPA628, peroxisomes accumulated in *pxdAΔ* hyphal tips, but EEs and nuclei were distributed normally (Fig. 1 A). To quantify peroxisome and EE distribution along hyphae, we performed line scans of fluorescence micrographs and plotted the average fluorescence intensity as a function of distance from the hyphal tip. The average peroxisome signal increased significantly in *pxdAΔ* hyphal tips, but no differences were observed in the average EE signal or position of the tip-proximal nucleus (Fig. 1 B). As an independent measurement of peroxisome distribution, we found that peroxisomes labeled with PexK (a homologue of *Saccharomyces cerevisiae* Pex11; Hynes et al., 2008) also accumulated in the hyphal tips of *pxdAΔ* strains (Fig. S1, C and D). We conclude that PxdA specifically regulates the distribution of peroxisomes, but not EEs or nuclei.

Peroxisome distribution and motility in *A. nidulans* requires the microtubule-based motors cytoplasmic dynein/NudA and kinesin-3a/UncA (Egan et al., 2012a,b). To determine whether the loss of *pxdA* affects peroxisome motility and distribution, we imaged peroxisomes in wild-type (WT) and *pxdAΔ* strains. In WT hyphae, peroxisomes exhibit both long-range runs and oscillatory movements (Video 1). In WT hyphae, 12% (n = 486) of peroxisomes exhibit long-range movements (distances >3 µm), consistent with previous studies in mammalian cells in which only 10%–15% of peroxisomes are motile (Rapp et al., 1996; Bharti et al., 2011). These long-range movements are reduced by >90% in *pxdAΔ* hyphae (Fig. 1, C and D; and Video 2). Furthermore, the velocity and run length of the small pool of peroxisomes that move in *pxdAΔ* hyphae are also reduced compared with WT (Figs. 1 E and S1 E). In contrast, the flux and velocity of EEs are similar in WT and *pxdAΔ* strains (Fig. 1, F–H; and Videos 3 and 4).

Taken together, our findings demonstrate that PxdA is required for the proper distribution and long-range movement of peroxisomes, but it is not required for the distribution or motility of EEs or nuclei. Our data also suggest that PxdA is not a core component of the transport machinery because deletions of this type would be predicted to result in defects in the transport or distribution of EEs and nuclei as well. Consistent with this, we find that the localization of dynein, characteristically seen as "comets" near the microtubule-plus end (Xiang et al., 2000), is intact in *pxdAΔ* hyphae (Fig. S1 F).

Peroxisomal hitchhiking on EEs is mediated by PxdA

Because PxdA is essential for peroxisome movement, we hypothesized that it might colocalize with moving peroxisomes. To visualize PxdA, we tagged the endogenous copy at its C terminus with either TagGFP (referred to as "GFP" from here on) or the red fluorescent protein mKate. C-terminal tagging of PxdA did not disrupt its function because line-scan analysis revealed that PxdA-GFP hyphae have normal peroxisome distribution (Fig. S2 A). In time-lapse videos, PxdA exhibits rapid bidirectional movement along the entire length of hyphae (Video 5). Kymograph analysis reveals that the velocity of PxdA is consistent with that of microtubule-based movement (Fig. 2, A and B). To evaluate the role of microtubules directly, we treated the PxdA-GFP strain with benomyl, a drug that inhibits microtubule polymerization and dynamic instability. The flux of bidirectional PxdA movements is largely abolished in benomyl- versus DMSO-treated conditions (Fig. 2 C). In contrast, we found no defects in PxdA flux in the presence of the actin polymerization inhibitor, latrunculin A (Fig. 2 C).

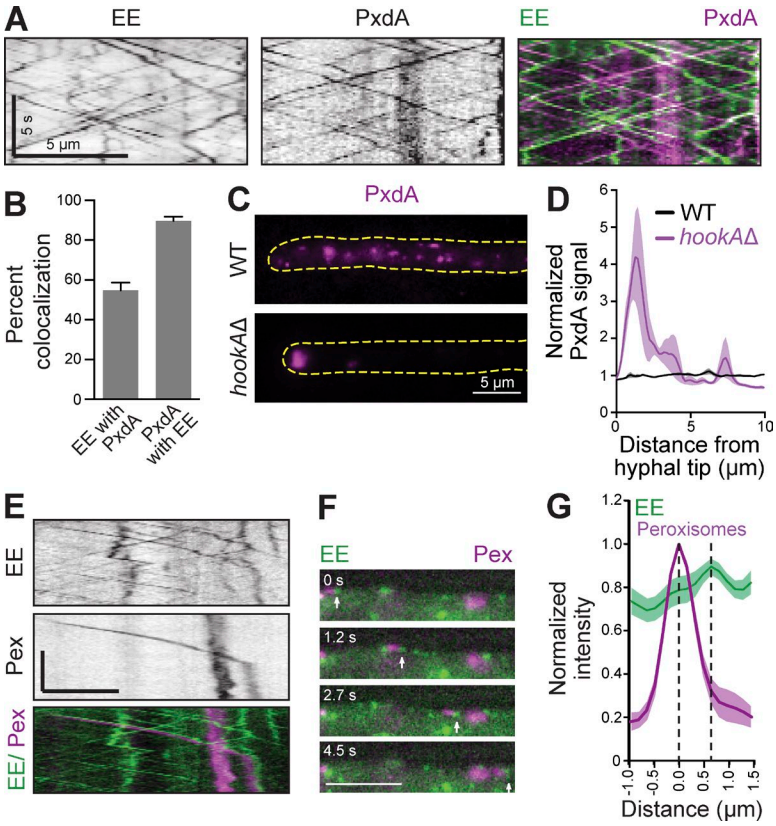

Figure 3. **EEs colocalize with PxdA and moving peroxisomes.** (A) Representative kymographs generated from simultaneous time-lapse movies of PxdA-mKate and GFP-RabA/5a–labeled EEs. (B) Bar graph quantifying the colocalization of PxdA-mKate and EEs. EEs colocalized with 54.8% ± 3.8% (SEM) PxdA puncta (n = 20 kymographs from 10 cells). PxdA colocalized with 89.7% ± 2.0% EEs (n = 20 kymographs from 10 cells). (C) Representative micrographs of PxdA-mKate distribution in WT versus *hookAΔ* hyphae. (D) Normalized line scans of WT and *hookAΔ* hyphae ($P < 0.0001$, two-way analysis of variance, Bonferroni post hoc test significant between 0.64 and 1.92 µm; n = 5 hyphae per genotype). (E) A kymograph generated from a simultaneous time-lapse movie of peroxisomes (pex) and EEs. 71.4% of moving peroxisomes (n = 28) overlapped with EEs. Bars: (x axis) 5 µm; (y axis) 5 s. (F) Stills from Video 8 of peroxisomes (Pex) and EEs. White arrows point to a co-migrating EE and peroxisome. Bar, 5 µm. (G) Normalized intensity line scans of peroxisomes and EEs during comigrating runs (n = 11).

To determine whether PxdA colocalizes with peroxisomes, we next visualized PxdA and peroxisomes simultaneously using dual-color time-lapse imaging. Kymograph analysis (Fig. 2 D) of time-lapse movies (Fig. 2 E and Video 6) revealed that 66% (n = 29) of moving peroxisomes co-migrate with PxdA. PxdA is rarely associated with stationary peroxisomes. Closer inspection of the time-lapse movies and kymographs revealed that PxdA localizes at the leading edge of moving peroxisomes with the peak PxdA signal leading by 560 ± 80 nm (mean ± SEM; Fig. 2 F). We also occasionally observed instances in which a moving PxdA puncta paused at a nonmotile peroxisome, an event that was followed by the movement of comigrating PxdA and the peroxisome (Fig. 2 D, middle and right).

Because we observed many more moving PxdA puncta than moving peroxisomes, and because PxdA motility was reminiscent of EE motility (Abenza et al., 2009; Zhang et al., 2010; Egan et al., 2012b, 2015), we next asked whether PxdA also colocalizes with EEs. To test this, we analyzed kymographs from simultaneous time-lapse movies of labeled PxdA and EEs (Video 7). Ninety percent of PxdA puncta colocalize with EEs, but only 55% of EEs colocalize with PxdA puncta (Fig. 3, A and B), demonstrating that PxdA is found on a subset of EEs.

We next sought to determine whether perturbing EE localization also perturbed PxdA localization. HookA has recently been identified as a cargo adaptor between EEs and dynein and kinesin-3 in filamentous fungi (Bielska et al., 2014; Zhang et al., 2014), and its vertebrate homolog (Hook3) is an activator of dynein/dynactin (McKenney et al., 2014). In the absence of HookA, EEs accumulate near the hyphal tip (Zhang et al., 2014). We reasoned that if most PxdA protein is associated with EEs, PxdA would accumulate at hyphal tips in *hookAΔ* strains. Indeed, we find that PxdA accumulates at the hyphal tip in *hookAΔ* compared with WT strains (Fig. 3, C and D), suggesting that PxdA is present on EEs that require HookA for motility.

The association between PxdA and EEs is somewhat surprising given that PxdA does not affect the motility or distribution of EEs (Fig. 1). Because PxdA colocalizes with a subset of EEs and moving peroxisomes, we next asked if EEs colocalized with moving peroxisomes. Kymograph analysis (Fig. 3 E) of time-lapse movies (Fig. 3 F and Video 8) reveals that 71% (n = 28) of moving peroxisomes colocalize with EEs, correlating well with the percentage of PxdA that colocalizes with moving peroxisomes (66%). In addition, similar to PxdA, EEs colocalized at the leading edge of moving peroxisomes (Fig. 3 F and Video 8). The peak EE signal was leading the peak peroxisome signal by 610 ± 170 nm (Fig. 3 G), comparable with what we observed for peroxisomes and PxdA (Fig. 2 F).

These results suggest that peroxisomes move by "hitchhiking" on EEs and that this process is mediated by PxdA. The concept that cellular components can hitchhike on EEs has been observed in *U. maydis* for Rrm4-containing ribonucleoprotein complexes (Baumann et al., 2012) and polysomes (Higuchi et al., 2014). In a study parallel to ours, also in *U. maydis*, peroxisomes, endoplasmic reticulum, and lipid droplets were observed to hitchhike on EEs (Guimaraes et al., 2015).

Endosomal localization of PxdA is required for peroxisome hitchhiking

We hypothesized that PxdA tethers EEs to peroxisomes to promote hitchhiking. If this were the case, we might be able to separate PxdA's EE localization from its function in peroxisome motility. To test this, we constructed a series of PxdA mutants (Fig. 4 A).

First, we sought to determine which domains of PxdA are necessary and sufficient for peroxisome motility. PxdA encodes a 2236-aa protein containing an ∼600-aa stretch of predicted

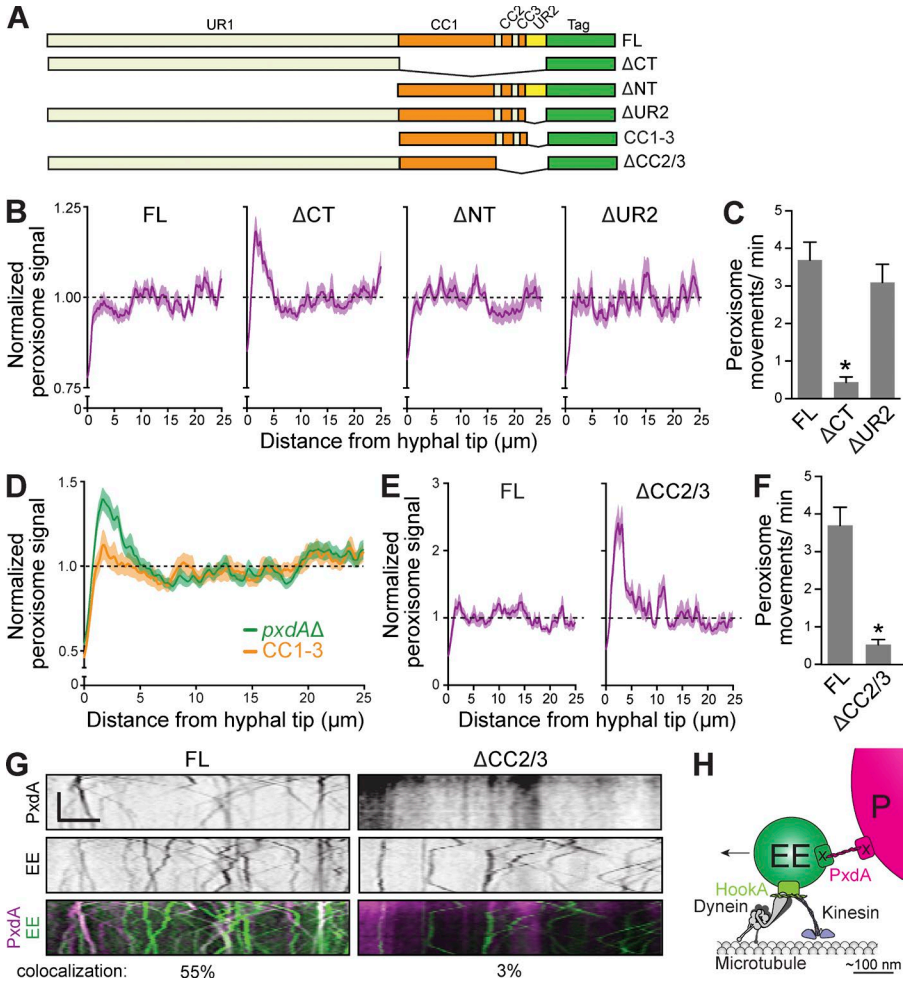

Figure 4. **Coiled-coil region of PxdA is necessary and sufficient for peroxisome motility and endosomal hitchhiking.** (A) Schematic of PxdA protein constructs used in this analysis relative to FL PxdA. UR1 (white) and UR2 (yellow) are on the N and C terminus, respectively. Predicted regions of coiled-coil (CC1, 2, and 3) are indicated in orange. All strains contain a C-terminal fluorescent protein tag (either mKate or TagGFP). (B) Normalized line scans of peroxisome distribution from the hyphal tip for FL, C-terminal deletion (ΔCT), N-terminal deletion (ΔNT), and ΔUR2 PxdA strains ($P < 0.0001$, two-way analysis of variance, Bonferroni post hoc test significant between 0.51 and 3.71 µm for FL vs. ΔCT; $n = 51–54$ hyphae per genotype). (C) Bar graph of the flux of peroxisome movements in FL, ΔCT, and ΔUR2 hyphae. Peroxisome movements were 3.69 ± 0.47 (SEM)/min for FL, 0.44 ± 0.14/min for ΔCT, and 3.10 ± 0.50/min for ΔUR2 ($P < 0.0001$, one-way analysis of variance; *, Bonferroni post hoc test significant for FL vs. ΔCT; FL vs. ΔUR2 was not significantly different; $n = 29–35$ hyphae per genotype). (D) Normalized line scans of peroxisome distribution along hyphae expressing either FL or CC1–3 PxdA ($P < 0.0001$, two-way analysis of variance, Bonferroni post hoc test significant between 1.19 and 3.03 µm from hyphal tip; $n = 78$ [FL] and $n = 68$ [CC1–3]). (E) Normalized line scans of peroxisome distribution along hyphae expressing either FL or ΔCC2/3 PxdA ($P < 0.0001$, two-way analysis of variance, Bonferroni post hoc test significant between 0.87 and 4.11 µm from hyphal tip; $n = 28$ [FL] and $n = 32$ [ΔCC2/3]). (F) Bar graph of the flux of peroxisome movements in FL and ΔCC2/3 hyphae. Peroxisome movements were 3.69 ± 0.47 (SEM) per min for FL (this is the same FL data depicted in C) and 0.51 ± 0.13 per min for ΔCC2/3 ($P < 0.0001$, one-way analysis of variance; *, Bonferroni post hoc test significant for FL vs. ΔCC2/3; $n = 29–35$ hyphae per genotype). (G) Representative kymographs generated from simultaneous time-lapse movies of EEs with FL or ΔCC2/3 PxdA. Colocalization represents the number of EEs that colocalize with PxdA. FL is 54.8% ± 3.8% (Fig. 3 B) and ΔCC2/3 3.2% ± 1.3% ($n = 10$ kymographs). (H) Model for peroxisome (P) hitchhiking on EEs mediated by PxdA. HookA recruits the transport machinery to EEs. PxdA is required to tether EEs to peroxisomes and may have distinct binding partners (x) on each organelle. The arrow depicts the direction of movement.

tandem coiled-coil domains (CC1–3), flanked by a large N-terminal uncharacterized region (UR1) and a much smaller C-terminal uncharacterized region (UR2; Fig. 4 A). Initially, we truncated the entire N-terminal UR1 (ΔNT) or the entire C-terminal region, including CC1–3 and UR2 (ΔCT) or the UR2 region alone (ΔUR2). We performed peroxisome line scans and found that peroxisomes accumulated at the hyphal tip of ΔCT strains, but not full-length (FL), ΔUR2, or ΔNT strains (Fig. 4 B). The PxdA-ΔCT strain also had a significant reduction in the flux of peroxisome movements compared with the FL and ΔUR2 strains (Fig. 4 C).

This analysis suggested that only the tandem CC (CC1–3) of PxdA is required for peroxisome distribution and motility. To test this directly, we expressed PxdA's CC1–3 alone and quantified peroxisome distribution and flux along hyphae. CC1–3 is sufficient to rescue the defects in both peroxisome distribution and peroxisome flux observed in *pxdAΔ* hyphae (Figs. 4 D and S2 B). Furthermore, PxdA CC1–3 localizes to moving puncta that show velocity and flux similar to those of strains expressing FL PxdA (Fig. S2, C–E). These experiments show that CC1–3 is necessary and sufficient for PxdA's function on peroxisomes.

We next sought to identify the region of PxdA required for its localization to EEs. We constructed a PxdA-mKate strain lacking CC2 and CC3 (ΔCC2/3; Fig. 4 A). Like PxdA ΔCT strains, PxdA ΔCC2/3 strains displayed an accumulation of peroxisomes at the hyphal tip (Fig. 4 E) and a severe drop in peroxisome flux (Fig. 4 F). In addition, PxdA ΔCC2/3-mKate had a diffuse signal in hyphae that was different from the EE localization observed for the FL protein, and only 3% of PxdA ΔCC2/3-mKate colocalized with EEs (Fig. 4 G). These data suggest that CC2/3 is critical for the EE localization of PxdA and that EE-linked PxdA is required for the proper distribution and movement of peroxisomes.

Overall, our study reveals that peroxisomes require PxdA to hitchhike on EEs for long-range movement. The abundance and rapid bidirectional movement of EEs in fungal hyphae make them a prime multifunctional platform for distributing a wide range of cargo (Göhre et al., 2012). In our model, HookA recruits the transport machinery to EEs (Zhang et al., 2014), and PxdA tethers peroxisomes to EEs (Fig. 4 H). The observation that both PxdA and EEs lead peroxisomes by ∼600 nm during movement (Figs. 2 E and 3 F) is consistent with the approximate diameter of peroxisomes (∼1 µm; Egan et al., 2012b) and

EEs (∼150 nm; Murk et al., 2003; Griffith et al., 2011). The size of PxdA's tandem coiled coil (CC1–3), which is predicted to be ∼90 nm, could easily bridge the distance between the peroxisome and EE. Interestingly, although there is no clear homologue of PxdA in mammalian species, a region of the coiled coil contains an F-bar domain (van Weering and Cullen, 2014) and is also weakly conserved with FKBP15, a protein known to associate with EEs in mammalian cells (Viklund et al., 2009). Exciting future directions include determining whether hitchhiking is broadly conserved outside of fungi, identifying the linkers required for other cargos to hitchhike on EEs, and determining the mechanisms that initiate and terminate hitchhiking.

Materials and methods

Fungal growth conditions

A. nidulans strains were grown in yeast extract and glucose medium (Szewczyk et al., 2006) or 1% glucose minimal medium (Nayak et al., 2006), supplemented with 1 mg/ml uracil, 2.4 mg/ml uridine, 2.5 µg/ml riboflavin, 1 µg/ml para-aminobenzoic acid, and 0.5 µg/ml pyridoxine when required. Glufosinate was used at a final concentration of 25 µl/ml as previously described (Nayak et al., 2006).

For imaging of germlings (for all organelle distribution experiments and CC1–3 flux experiments), spores were resuspended in 0.5 ml of 0.01% Tween-80 solution. The spore suspension was diluted at 1:1,000 in liquid minimal medium containing appropriate auxotrophic supplements. The spore and media mix (400 µl) was added to an eight-chambered Nunc Lab-Tek II coverglass (Thermo Fisher Scientific) and incubated at 30°C for 16–20 h before imaging. For imaging of mature hyphae (for velocity and flux experiments), spores were inoculated on minimal medium plates containing the appropriate auxotrophic supplements and incubated at 37°C for 12–16 h. Colonies were excised from agar plates and inverted on Lab-Tek plates for imaging. For benomyl and latrunculin A experiments, minimal media containing the drugs (2.4 µg/ml for benomyl [Sigma-Aldrich]; 12 µM for latrunculin A [Life Technologies]) or DMSO control (1.2%) were added fresh to Lab-Tek chambers containing germlings and were imaged 45 min to 1 h later. For Western blots, cells were grown in yeast extract and glucose medium for 16–20 h, strained in Miracloth (Millipore), and flash frozen in liquid nitrogen. For lysis, cells were ground in liquid nitrogen and boiled in 9 M urea denaturing buffer (125 mM Tris-HCl, pH 6.8, 9 M urea, 1 mM EDTA, pH 7.0, 4% SDS, 10 mM DTT, 10% β-mercaptoethanol, and 4% glycerol) before running on SDS-PAGE.

Strain construction

Strains of *A. nidulans* used in this study are listed in Table S1. All strains were confirmed by a combination of PCR and sequencing from genomic DNA isolated as previously described (Lee and Taylor, 1990). Strains were created by homologous recombination to replace the endogenous gene in strains lacking *ku70* (Nayak et al., 2006) with *Afribo* (*Aspergillus fumigatus Ribo*), *AfpyrG* (*Aspergillus fumigatus pyrG*), *Afpyro* (*Aspergillus fumigatus pyro*), or *bar* (Straubinger et al., 1992) as selectable markers. All linearized transforming DNA for deletion strains, including *pxdAΔ* and *hookAΔ*, were constructed by fusion PCR (Szewczyk et al., 2006). All PxdA DNA constructs contained a C-terminal codon-optimized fluorescent protein tag, either TagGFP2 (Subach et al., 2008) or mKate2 (Shcherbo et al., 2009), followed by *pxdA*'s native 3′ UTR, and were inserted into the Blue Heron Biotechnology pUC vector at 5′ EcoRI and 3′ HindIII restriction sites using isothermal assembly (Gibson et al., 2009). Plasmid constructs were confirmed by sequencing. Linearized transforming DNA from plasmid constructs was created by PCR with flanking primers located at the 5′ and 3′ ends of homologous arms.

The amino acid positions for each PxdA construct in Fig. 4 were as follows: FL, aa 1–2,236; ΔNT, aa 1,466–2,236; ΔCT, aa 1–1,465; ΔUR2, aa 1–2,116; and ΔCC2/3, aa 1–1,946. For the CC1–3 rescue experiment (Figs. 4 D and S1, B–D), the CC1–3 construct (aa 1,466–2,116) was inserted into a *pxdA*Δ strain at the endogenous locus.

Fluorescence microscopy

All images were collected at 22°C. For acquisition of the distribution and motility of peroxisomes (PTS1-mCherry and PexK-GFP) and for the distribution of EEs (GFP-RabA/5a), dynein (NudA-3xGFP), and PxdA, images were collected using a Plan Apo 60×/1.42 (Olympus) oil immersion objective on an epifluorescence Deltavision Core microscope (GE Healthcare). GFP was excited with a 488-nm laser line (50 mW) and collected with a 525/50 FITC emission filter. mCherry fluorescence was excited with the 561-nm laser line (50 mW) and collected with a 594/45 emission filter. Images were acquired with a PCO edge sCMOS camera (Kelkeim) and controlled with softWoRx software (GE Healthcare). For distribution images, 20 optical *z*-sections were collected with a step size of 0.5 µm. Hyphae (used for outlining cells) were imaged using brightfield.

Simultaneous multicolor time-lapse images were collected using a Plan Apo 60×/1.42 oil immersion objective on the Deltavision OMX Blaze V4 system (GE Healthcare). GFP and mKate2/mCherry were excited simultaneously with 488- and 568-nm diode laser lines (100 mW), respectively. A series of dichroic mirrors were used to split emission light from fluorophores to different PCO Edge sCMOS cameras. An emission filter in front of both cameras was used to select appropriate wavelengths (528/48 and 609/37 for GFP and mKate/mCherry, respectively). Images were aligned and registered using the OMX alignment slide and corrected for translation, rotation, and magnification differences between channels using softWoRx software. Some images were deconvolved using the enhanced ratio method (five iterations) and/or binned (2 × 2).

For EE and PxdA motility assays, time-lapse images were collected using a Plan Apochromat TIRF 100×/1.49 oil immersion objective on an epifluorescence Ti-E motorized inverted microscope (Nikon) with the Perfect focus system (Nikon) for continuous maintenance of focus, all controlled by NIS-Elements software (Nikon). GFP fluorescence was excited using a 488-nm laser line (50 mW) and collected with a 525/50 emission filter. Images were acquired with an EM-CCD camera (DU-897; Andor).

Images were brightness and contrast adjusted using ImageJ (version 2.0; National Institutes of Health) and Photoshop CS3 (version 10.0; Adobe), and figures were compiled in Illustrator CC (2015.2; Adobe).

Image and data analysis

For peroxisome, EE, and PxdA line-scan distribution measurements, maximum-intensity projections of fluorescence micrographs and brightfield images (for hyphae) were obtained using ImageJ. Brightfield images of hyphae were traced using the segmented line tool (line width 25), starting from the hyphal tip and ending at a point indicated in the *x* axis of respective line-scan graphs. Each trace was overlaid onto the corresponding fluorescence micrograph and used to project the average fluorescence intensity. For peroxisome normalization (Fig. 4), average intensity values at each point along hyphae were normalized against that particular condition's baseline mean (10–25 µm). For PxdA normalization (Fig. 3 D), average intensity values at each point along hyphae were normalized against that particular condition's baseline average (5–10 µm). For flux measurements, the number of puncta crossing a line 10 µm perpendicular to and from the hyphal tip was calculated (Egan et al., 2012b).

EE, peroxisome, and PxdA velocities and run lengths were measured using ImageJ. Maximum-intensity projections were generated from time-lapse sequences to define the trajectory of particles of interest. The segmented line tool was used to trace the trajectories and map them onto the original video sequence, which was subsequently resliced to generate a kymograph. The instantaneous velocities of individual movements (for runs ≥2 µm in length) were calculated from the inverse of the slopes of kymograph traces, and run-length measurements were obtained from each of these traces. For measurements of normalized intensity during co-migrating runs between PxdA or EEs with peroxisomes (Figs. 2 E and 3 F), peroxisomes and associated puncta (PxdA or EEs) were traced using ImageJ at a point along the trajectory of the path (in the direction of movement) that was clear and distinct from other puncta on the micrograph. Line intensity profiles for each channel individually were generated. The "0" along the *x* axis corresponds to the position of peak intensity for the peroxisome signal. Intensities for each channel were normalized to that channel's peak intensity for each comigrating run.

Data visualization and statistical analyses were performed using GraphPad Prism (6.0d; GraphPad Software), Excel (version 14.5.8; Microsoft), and ImageJ (2.0). Analysis of variance followed by Bonferroni post hoc statistical tests were used for all distribution comparisons, and nonparametric Mann-Whitney or Kolmogorov-Smirnov tests were used for all flux and velocity comparisons, respectively. All experiments were analyzed from at least three independent replicates, except for ΔCC2/3 experiments (Fig. 4, E–G) and CC1–3 flux/velocity measurements (Fig. S2, B, D, and E), which were analyzed from two independent replicates.

Online supplemental material

Fig. S1 shows that peroxisomes accumulate in the hyphal tip in PxdA mutant and deletion strains, but EEs, nuclei, and cytoplasmic dynein are unaffected. Fig. S2 shows that tagging PxdA does not affect its function and that expressing its CC alone moves similarly to the FL protein. Video 1 shows peroxisome dynamics in a WT hypha. Video 2 shows peroxisome dynamics are perturbed in a pxdAΔ hypha. Video 3 shows EE dynamics in a WT hypha. Video 4 shows that EE dynamics are unaffected in a *pxdA*Δ hypha. Video 5 shows PxdA-GFP dynamics in a hypha. Video 6 shows PxdA-GFP comigrating with a moving peroxisome. Video 7 shows PxdA-GFP colocalizing with EEs. Video 8 shows an EE comigrating with a moving peroxisome. Table S1 lists the *A. nidulans* strains used in this study. Online supplemental material is available at http://www.jcb.org/cgi/content/full/jcb.201512020/DC1. Additional data are available in the JCB DataViewer at http://dx.doi.org/10.1083/jcb.201512020.dv.

Acknowledgments

We thank the Reck-Peterson laboratory and Andres Leschziner for critical feedback on experiments and the manuscript. We thank Jennifer Waters, Talley Lambert, and The Nikon Imaging Center at Harvard Medical School for helpful technical advice and imaging training.

Early stages of this project were supported by a National Institutes of Health New Innovator award (OD004268) to S. Reck-Peterson and subsequent work by R01 GM 107214 to S. Reck-Peterson.

The authors declare no competing financial interests.

Submitted: 4 December 2015
Accepted: 5 January 2016

References

Abenza, J.F., A. Pantazopoulou, J.M. Rodríguez, A. Galindo, and M.A. Peñalva. 2009. Long-distance movement of *Aspergillus nidulans* early endosomes on microtubule tracks. *Traffic.* 10:57–75. http://dx.doi.org/10.1111/j.1600-0854.2008.00848.x

Baumann, S., T. Pohlmann, M. Jungbluth, A. Brachmann, and M. Feldbrügge. 2012. Kinesin-3 and dynein mediate microtubule-dependent co-transport of mRNPs and endosomes. *J. Cell Sci.* 125:2740–2752. http://dx.doi.org/10.1242/jcs.101212

Bharti, P., W. Schliebs, T. Schievelbusch, A. Neuhaus, C. David, K. Kock, C. Herrmann, H.E. Meyer, S. Wiese, B. Warscheid, et al. 2011. PEX14 is required for microtubule-based peroxisome motility in human cells. *J. Cell Sci.* 124:1759–1768. http://dx.doi.org/10.1242/jcs.079368

Bielska, E., M. Schuster, Y. Roger, A. Berepiki, D.M. Soanes, N.J. Talbot, and G. Steinberg. 2014. Hook is an adapter that coordinates kinesin-3 and dynein cargo attachment on early endosomes. *J. Cell Biol.* 204:989–1007. http://dx.doi.org/10.1083/jcb.201309022

Cianfrocco, M.A., M.E. DeSantis, A.E. Leschziner, and S.L. Reck-Peterson. 2015. Mechanism and regulation of cytoplasmic dynein. *Annu. Rev. Cell Dev. Biol.* 31:83–108. http://dx.doi.org/10.1146/annurev-cellbio-100814-125438

Egan, M.J., M.A. McClintock, and S.L. Reck-Peterson. 2012a. Microtubule-based transport in filamentous fungi. *Curr. Opin. Microbiol.* 15:637–645. http://dx.doi.org/10.1016/j.mib.2012.10.003

Egan, M.J., K. Tan, and S.L. Reck-Peterson. 2012b. Lis1 is an initiation factor for dynein-driven organelle transport. *J. Cell Biol.* 197:971–982. http://dx.doi.org/10.1083/jcb.201112101

Egan, M.J., M.A. McClintock, I.H. Hollyer, H.L. Elliott, and S.L. Reck-Peterson. 2015. Cytoplasmic dynein is required for the spatial organization of protein aggregates in filamentous fungi. *Cell Reports.* 11:201–209. http://dx.doi.org/10.1016/j.celrep.2015.03.028

Fu, M.M., and E.L. Holzbaur. 2014. Integrated regulation of motor-driven organelle transport by scaffolding proteins. *Trends Cell Biol.* 24:564–574. http://dx.doi.org/10.1016/j.tcb.2014.05.002

Gibson, D.G., L. Young, R.Y. Chuang, J.C. Venter, C.A. Hutchison III, and H.O. Smith. 2009. Enzymatic assembly of DNA molecules up to several hundred kilobases. *Nat. Methods.* 6:343–345. http://dx.doi.org/10.1038/nmeth.1318

Glater, E.E., L.J. Megeath, R.S. Stowers, and T.L. Schwarz. 2006. Axonal transport of mitochondria requires milton to recruit kinesin heavy chain and is light chain independent. *J. Cell Biol.* 173:545–557. http://dx.doi.org/10.1083/jcb.200601067

Göhre, V., E. Vollmeister, M. Bölker, and M. Feldbrügge. 2012. Microtubule-dependent membrane dynamics in *Ustilago maydis*: Trafficking and function of Rab5a-positive endosomes. *Commun. Integr. Biol.* 5:485–490. http://dx.doi.org/10.4161/cib.21219

Griffith, J., M.A. Peñalva, and F. Reggiori. 2011. Adaptation of the Tokuyasu method for the ultrastructural study and immunogold labelling of filamentous fungi. *J. Electron Microsc. (Tokyo).* 60:211–216. http://dx.doi.org/10.1093/jmicro/dfr026

Guimaraes, S.C., M. Schuster, E. Bielska, G. Dagdas, S. Kilaru, B.R. Meadows, M. Schrader, and G. Steinberg. 2015. Peroxisomes, lipid droplets, and endoplasmic reticulum "hitchhike" on motile early endosomes. *J. Cell Biol.* 211:945–954. http://dx.doi.org/10.1083/jcb.201505086

Harada, A., Y. Takei, Y. Kanai, Y. Tanaka, S. Nonaka, and N. Hirokawa. 1998. Golgi vesiculation and lysosome dispersion in cells lacking cytoplasmic dynein. *J. Cell Biol.* 141:51–59. http://dx.doi.org/10.1083/jcb.141.1.51

Higuchi, Y., P. Ashwin, Y. Roger, and G. Steinberg. 2014. Early endosome motility spatially organizes polysome distribution. *J. Cell Biol.* 204:343–357. http://dx.doi.org/10.1083/jcb.201307164

Horio, T., and B.R. Oakley. 2005. The role of microtubules in rapid hyphal tip growth of *Aspergillus nidulans*. *Mol. Biol. Cell.* 16:918–926. http://dx.doi.org/10.1091/mbc.E04-09-0798

Hynes, M.J., S.L. Murray, G.S. Khew, and M.A. Davis. 2008. Genetic analysis of the role of peroxisomes in the utilization of acetate and fatty acids in Aspergillus nidulans. *Genetics.* 178:1355–1369. http://dx.doi.org/10.1534/genetics.107.085795

Kardon, J.R., and R.D. Vale. 2009. Regulators of the cytoplasmic dynein motor. *Nat. Rev. Mol. Cell Biol.* 10:854–865. http://dx.doi.org/10.1038/nrm2804

Kural, C., H. Kim, S. Syed, G. Goshima, V.I. Gelfand, and P.R. Selvin. 2005. Kinesin and dynein move a peroxisome in vivo: a tug-of-war or coordinated movement? *Science.* 308:1469–1472. http://dx.doi.org/10.1126/science.1108408

Lee, S.B., and J.W. Taylor. 1990. Isolation of DNA from fungal mycelia and single spores. In PCR Protocols: A Guide to Methods and Applications.

M. Innis, D. Gelfand, J. Sninsky, and T. White, editors. Academic Press, Orlando, FL. 282–287.

Liu, F., S.K. Ng, Y. Lu, W. Low, J. Lai, and G. Jedd. 2008. Making two organelles from one: Woronin body biogenesis by peroxisomal protein sorting. *J. Cell Biol.* 180:325–339. http://dx.doi.org/10.1083/jcb.200705049

Maday, S., and E.L. Holzbaur. 2012. Autophagosome assembly and cargo capture in the distal axon. *Autophagy.* 8:858–860. http://dx.doi.org/10.4161/auto.20055

McKenney, R.J., W. Huynh, M.E. Tanenbaum, G. Bhabha, and R.D. Vale. 2014. Activation of cytoplasmic dynein motility by dynactin-cargo adapter complexes. *Science.* 345:337–341. http://dx.doi.org/10.1126/science.1254198

Murk, J.L., G. Posthuma, A.J. Koster, H.J. Geuze, A.J. Verkleij, M.J. Kleijmeer, and B.M. Humbel. 2003. Influence of aldehyde fixation on the morphology of endosomes and lysosomes: quantitative analysis and electron tomography. *J. Microsc.* 212:81–90. http://dx.doi.org/10.1046/j.1365-2818.2003.01238.x

Nayak, T., E. Szewczyk, C.E. Oakley, A. Osmani, L. Ukil, S.L. Murray, M.J. Hynes, S.A. Osmani, and B.R. Oakley. 2006. A versatile and efficient gene-targeting system for *Aspergillus nidulans*. *Genetics.* 172:1557–1566. http://dx.doi.org/10.1534/genetics.105.052563

Neuhaus, A., C. Eggeling, R. Erdmann, and W. Schliebs. 2015. Why do peroxisomes associate with the cytoskeleton?. *Biochim. Biophys. Acta.* http://dx.doi.org/10.1016/j.bbamcr.2015.11.022

Rapp, S., R. Saffrich, M. Anton, U. Jäkle, W. Ansorge, K. Gorgas, and W.W. Just. 1996. Microtubule-based peroxisome movement. *J. Cell Sci.* 109:837–849.

Roghi, C., and V.J. Allan. 1999. Dynamic association of cytoplasmic dynein heavy chain 1a with the Golgi apparatus and intermediate compartment. *J. Cell Sci.* 112:4673–4685.

Schrader, M., S.J. King, T.A. Stroh, and T.A. Schroer. 2000. Real time imaging reveals a peroxisomal reticulum in living cells. *J. Cell Sci.* 113:3663–3671.

Shcherbo, D., C.S. Murphy, G.V. Ermakova, E.A. Solovieva, T.V. Chepurnykh, A.S. Shcheglov, V.V. Verkhusha, V.Z. Pletnev, K.L. Hazelwood, P.M. Roche, et al. 2009. Far-red fluorescent tags for protein imaging in living tissues. *Biochem. J.* 418:567–574. http://dx.doi.org/10.1042/BJ20081949

Straubinger, B., E. Straubinger, S. Wirsel, G. Turgeon, and O.C. Yoder. 1992. Versitile fungal transformation vectors carrying the selectable bar gene of *Streptomyces hygroscopicus*. *Fungal Genetics Newsletter* 39:82–83.

Subach, O.M., I.S. Gundorov, M. Yoshimura, F.V. Subach, J. Zhang, D. Grüenwald, E.A. Souslova, D.M. Chudakov, and V.V. Verkhusha. 2008. Conversion of red fluorescent protein into a bright blue probe. *Chem. Biol.* 15:1116–1124. http://dx.doi.org/10.1016/j.chembiol.2008.08.006

Szewczyk, E., T. Nayak, C.E. Oakley, H. Edgerton, Y. Xiong, N. Taheri-Talesh, S.A. Osmani, and B.R. Oakley. 2006. Fusion PCR and gene targeting in *Aspergillus nidulans*. *Nat. Protoc.* 1:3111–3120. http://dx.doi.org/10.1038/nprot.2006.405

Tan, K., A.J. Roberts, M. Chonofsky, M.J. Egan, and S.L. Reck-Peterson. 2014. A microscopy-based screen employing multiplex genome sequencing identifies cargo-specific requirements for dynein velocity. *Mol. Biol. Cell.* 25:669–678. http://dx.doi.org/10.1091/mbc.E13-09-0557

Tanaka, Y., Y. Kanai, Y. Okada, S. Nonaka, S. Takeda, A. Harada, and N. Hirokawa. 1998. Targeted disruption of mouse conventional kinesin heavy chain, kif5B, results in abnormal perinuclear clustering of mitochondria. *Cell.* 93:1147–1158. http://dx.doi.org/10.1016/S0092-8674(00)81459-2

Vale, R.D. 2003. The molecular motor toolbox for intracellular transport. *Cell.* 112:467–480. http://dx.doi.org/10.1016/S0092-8674(03)00111-9

van Spronsen, M., M. Mikhaylova, J. Lipka, M.A. Schlager, D.J. van den Heuvel, M. Kuijpers, P.S. Wulf, N. Keijzer, J. Demmers, L.C. Kapitein, et al. 2013. TRAK/Milton motor-adaptor proteins steer mitochondrial trafficking to axons and dendrites. *Neuron.* 77:485–502. http://dx.doi.org/10.1016/j.neuron.2012.11.027

van Weering, J.R., and P.J. Cullen. 2014. Membrane-associated cargo recycling by tubule-based endosomal sorting. *Semin. Cell Dev. Biol.* 31:40–47. http://dx.doi.org/10.1016/j.semcdb.2014.03.015

Viklund, I.M., P. Aspenström, V. Meas-Yedid, B. Zhang, J. Kopec, D. Agren, G. Schneider, M. D'Amato, J.C. Olivo-Marin, P. Sansonetti, et al. 2009. WAFL, a new protein involved in regulation of early endocytic transport at the intersection of actin and microtubule dynamics. *Exp. Cell Res.* 315:1040–1052. http://dx.doi.org/10.1016/j.yexcr.2008.12.004

Wang, X., and T.L. Schwarz. 2009. The mechanism of Ca2+-dependent regulation of kinesin-mediated mitochondrial motility. *Cell.* 136:163–174. http://dx.doi.org/10.1016/j.cell.2008.11.046

Wedlich-Söldner, R., A. Straube, M.W. Friedrich, and G. Steinberg. 2002. A balance of KIF1A-like kinesin and dynein organizes early endosomes in the fungus *Ustilago maydis*. *EMBO J.* 21:2946–2957. http://dx.doi.org/10.1093/emboj/cdf296

Xiang, X., S.M. Beckwith, and N.R. Morris. 1994. Cytoplasmic dynein is involved in nuclear migration in *Aspergillus nidulans*. *Proc. Natl. Acad. Sci. USA.* 91:2100–2104. http://dx.doi.org/10.1073/pnas.91.6.2100

Xiang, X., G. Han, D.A. Winkelmann, W. Zuo, and N.R. Morris. 2000. Dynamics of cytoplasmic dynein in living cells and the effect of a mutation in the dynactin complex actin-related protein Arp1. *Curr. Biol.* 10:603–606. http://dx.doi.org/10.1016/S0960-9822(00)00488-7

Zhang, J., L. Zhuang, Y. Lee, J.F. Abenza, M.A. Peñalva, and X. Xiang. 2010. The microtubule plus-end localization of *Aspergillus* dynein is important for dynein-early-endosome interaction but not for dynein ATPase activation. *J. Cell Sci.* 123:3596–3604. http://dx.doi.org/10.1242/jcs.075259

Zhang, J., R. Qiu, H.N. Arst Jr., M.A. Peñalva, and X. Xiang. 2014. HookA is a novel dynein-early endosome linker critical for cargo movement in vivo. *J. Cell Biol.* 204:1009–1026. http://dx.doi.org/10.1083/jcb.201308009